arXiv:2105.02705v1 [cond-mat.mtrl-sci] 6 May 2021

Growth and Characterisation Studies of Eu_3O_4 Thin Films Grown on Si/SiO_2 and Graphene

R. O. M. Aboljadayel,[1,2,*] A. Ionescu,[1] O. J. Burton,[3]
G. Cheglakov,[1] S. Hofmann,[3] and C. H. W. Barnes[1]

[1]*Cavendish Laboratory, Physics Department,*
University of Cambridge, Cambridge CB3 0HE, United Kingdom.
[2]*Diamond Light Source, Didcot, OX11 0DE, UK*
[3]*Department of Engineering, University of Cambridge,*
Cambridge CB3 0FA, United Kingdom.

(Dated: January 7, 2022)

Abstract

We report the growth, structural and magnetic properties of the less studied Eu-oxide phase, Eu_3O_4, thin films grown on a Si/SiO_2 substrate and Si/SiO_2/graphene using molecular beam epitaxy. The X-ray diffraction scans show that highly-textured crystalline $Eu_3O_4(001)$ films are grown on both substrates, whereas the film deposited on graphene has a better crystallinity than that grown on the Si/SiO_2 substrate. The SQUID measurements show that both films have a Curie temperature of 5.5 ± 0.1 K, with a magnetic moment of 0.0032 emu/g at 2 K. The mixed-valency of the Eu cations has been confirmed by the qualitative analysis of the depth-profile X-ray photoelectron spectroscopy measurements with the Eu^{2+} : Eu^{3+} ratio of 28 : 72. However, surprisingly, our films show no metamagnetic behaviour as reported for the bulk and powder form. Furthermore, the Raman spectroscopy scans show that the growth of the Eu_3O_4 thin films has no damaging effect on the underlayer graphene sheet. Therefore, the graphene layer is expected to retain its properties.

I. INTRODUCTION

Mixed-valence or fluctuating valence behaviour are usually found in lanthanide-based compounds due to the intermixing of the $s-d$ band with the localised f band near the Fermi level. Therefore, they exhibit unique magnetic, thermal and electrical properties [1]. Eu cations in Eu-based compounds mostly occur in the 2^+ valence. However, in trieuropium tetroxide (Eu_3O_4) Eu ions exhibit a mixed-valence of Eu^{2+} and Eu^{3+}.

Eu_3O_4 crystallises into an orthorhombic structure (space group *Pnma*) similar to $CaFe_2O_4$ with the lattice parameters a= 10.085 Å, b= 3.502 Å and c= 12.054 Å [2, 3]. Figure 1 shows the Eu_3O_4 structure, where the Eu^{2+} and Eu^{3+} ions are occupying the Ca^{2+} and Fe^{3+} sites, respectively. The oxygen ions form a six- and eight-fold coordination around the Eu^{3+} and Eu^{2+} ions, respectively. The coordination is then completed with two oxygen ions lying at the corner of the crystal [2, 4]. Therefore, Eu_3O_4 has two Eu^{3+} and one Eu^{2+} ions per unit formula [4].

The compound Eu_3O_4 has an antiferromagnetic arrangement below 5 K. Its bulk and powder forms show a metamagnetic behaviour below the Néel temperature (T_N), at a crit-

* roma2@cam.ac.uk; razan.aboljadayel@diamond.ac.uk

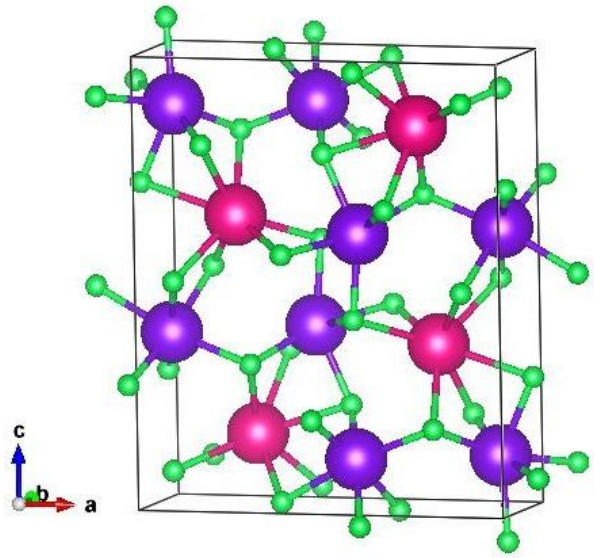


FIG. 1. The orthorhombic structure of Eu_3O_4, in which the purple, magenta and green spheres represent the Eu^{3+}, Eu^{2+} and O^{2-} ions, respectively. The black box represents one unit cell of the Eu_3O_4 crystal.

ical field of 2.4 kOe. Therefore, Eu_3O_4 is considered a potential material for magnetic refrigeration applications [3–5]. Although Eu_3O_4 is a mixed-valence compound, its magnetic ordering is mainly determined by the Eu^{2+} ions at low-temperature due to the high magnetic moment of Eu^{2+} (total angular momentum, $J= 7/2$) in comparison to the Eu^{3+} ions ($J= 0$) [3–5]. It has been proposed that the nearest neighbouring Eu^{2+} ions are strongly coupled by ferromagnetic interactions at low temperature, whereas the distant ions are coupled by weaker antiferromagnetic coupling, resulting in the overall antiferromagnetic state of Eu_3O_4 [5].

Graphene is a promising material for spintronics applications due to its desirable properties such as its long spin-diffusion length and high electron mobility. So far, no study on the graphene/Eu_3O_4 system has been reported. This may well be due to the difficulty of growing Eu_3O_4, which is the unstable high-temperature phase of Eu-oxides. Therefore, this study presents one of the first fundamental steps towards understanding the exchange coupling between a Eu_3O_4 and graphene.

In this study, 20 nm Eu_3O_4 thick films were grown on a Si/SiO_2 substrate and graphene sheet supported on Si/SiO_2 by molecular beam epitaxy (MBE) and capped with 5 nm of Au. Eu was deposited at high temperatures (300 - 600 °C) in an oxygen flux. The growth

parameters such as the oxygen partial pressure, temperature and deposition rate were optimised to achieve a crystalline $Eu_3O_4(001)$ phase. The structural characterisation of the films was studied by X-ray diffraction (XRD) and reflection (XRR), where a superconducting quantum interference device magnetometer (SQUID) was used to study their magnetic properties. The results show a successful growth of crystalline, highly-textured Eu_3O_4 (001) films with a Curie temperature (T_C) of $\sim$ 5 K, which is in agreement with the value reported in Ref. [3]. Depth-profile X-ray photon electron spectroscopy (XPS) scans were performed to prove the mixed-valence of Eu cations in Eu_3O_4. Furthermore, Raman spectroscopy measurements on the Si/SiO_2/graphene/Eu_3O_4 sample showed that although the growth of Eu_3O_4 film induced defects in the graphene sheet, the graphene retains its hexagonal lattice structure.

II. SAMPLE PREPARATION

20 nm $Eu_3O_4(001)$ films were deposited on cleaned Si/SiO_2 and commercially purchased Si/SiO_2/graphene substrates by MBE with a base pressure of 4×10^{-10} mbar. The substrates were heated to 400°C, while the Eu was evaporated at a rate of 1.2 nm/min. Oxygen was then introduced into the growth chamber, resulting in a partial pressure of 1.1×10^{-8} mbar to deposit $Eu_3O_4(001)$ at a rate of 1.11 nm/min. A 5 nm film of Au was grown subsequently on the $Eu_3O_4(001)$ films to prevent them from oxidising to the most stable oxide phase of Eu (Eu_2O_3). The Au films were deposited at 45°C, with a rate of 0.057 nm/min at a pressure of 1.9×10^{-10} mbar.

A quartz crystal microbalance was used during the deposition to monitor the growth rate and thus the thicknesses of the layers. Room temperature (RT) XRD scans were used to study the crystallinity of the grown films. The XRR measurements were then performed to confirm the results of the microbalance readings and deduce the density and roughness between the layers. These acquisitions were carried out using a Bruker D8 Discover HRXRD with a Cu Kα monochromatic beam with a voltage of 40 kV and a current of 40 mA. The magnetic properties of the Eu_3O_4 films were studied using a Quantum Design SQUID.

Depth-profile XPS scans using Al Kα X-ray source (1486.68 eV, beam width of 500 μm) were performed on the $Si/SiO_2/Eu_3O_4$/Au sample. This was done to study the homogeneity of the Eu_3O_4 film, determine the atomic ratio of Eu^{2+} and Eu^{3+} and confirm the mixed-

valence character of the grown film. Furthermore, the effect of depositing Eu_3O_4 film on the graphene sheet was investigated by Raman spectroscopy measurements using a Renishaw InVia spectrometer (100× objective, 10% laser power, spot size of $\sim 1\,\mu$m, 0.5 s exposure time, a wavelength of 532 nm). However, the Au capping layer was selectively etched in KI/I_2 solution before the measurements to eliminate the Au interference with the Raman measurements. The Si/SiO_2/graphene/Eu_3O_4/Au sample was cleaved into $\sim 2 \times 2$ mm square and placed in the etchant solution for 5 minutes at RT, rinsed with DI water twice, then with IPA and dried with dry N_2. Raman scans were then taken at every $50\,\mu$m in a grid pattern over an area of $1000\,\mu$m $\times 1000\,\mu$m for the region coated with Eu_3O_4, and every $10\,\mu$m over an area of $140\,\mu$m $\times 140\,\mu$m for the bare graphene surface.

III. RESULTS AND DISCUSSION

A. X-ray Diffraction (XRD)

The RT XRD scans (from 20° - 100°) of the $Eu_3O_4(001)$ films grown on the Si/SiO_2 substrate and on graphene are shown in Figure 2 (a). The XRD scans show highly textured $Eu_3O_4(002)$ films with no sign of other oxide-phase of Eu or unreacted Eu within the detection limit of the set-up. Additional $Eu_3O_4(004)$ and (008) peaks are observed in the scan of the Si/SiO_2/graphene/Eu_3O_4/Au sample, indicating that the underlying graphene layer improves the crystallinity of the Eu_3O_4 film. This is also proven by the smaller full-width at half-maximum (FWHM) of the Eu_3O_4 peaks of the Si/SiO_2/graphene/Eu_3O_4/Au sample compared to the Si/SiO_2/Eu_3O_4/Au. Figure 2 (b) shows the XRR scan and the corresponding fit for the Si/SiO_2/Eu_3O_4/Au sample, whereas the deduced values for the thickness, density and roughness of the layers are listed in the inset table.

B. SQUID

Figure 3 shows the field-cooled (FC) and zero field-cooled (ZFC) measurements of the Si/SiO_2/$Eu_3O_4(001)$/Au and Si/SiO_2/graphene/$Eu_3O_4(001)$/Au samples, respectively. Both show a T_C of $\sim 5.5 \pm 0.1$ K as can be deduced from the $\mathrm{d}M/\mathrm{d}T$ vs T (insets), which agrees with values reported in the literature [3–5]. Therefore, care has to be given to check

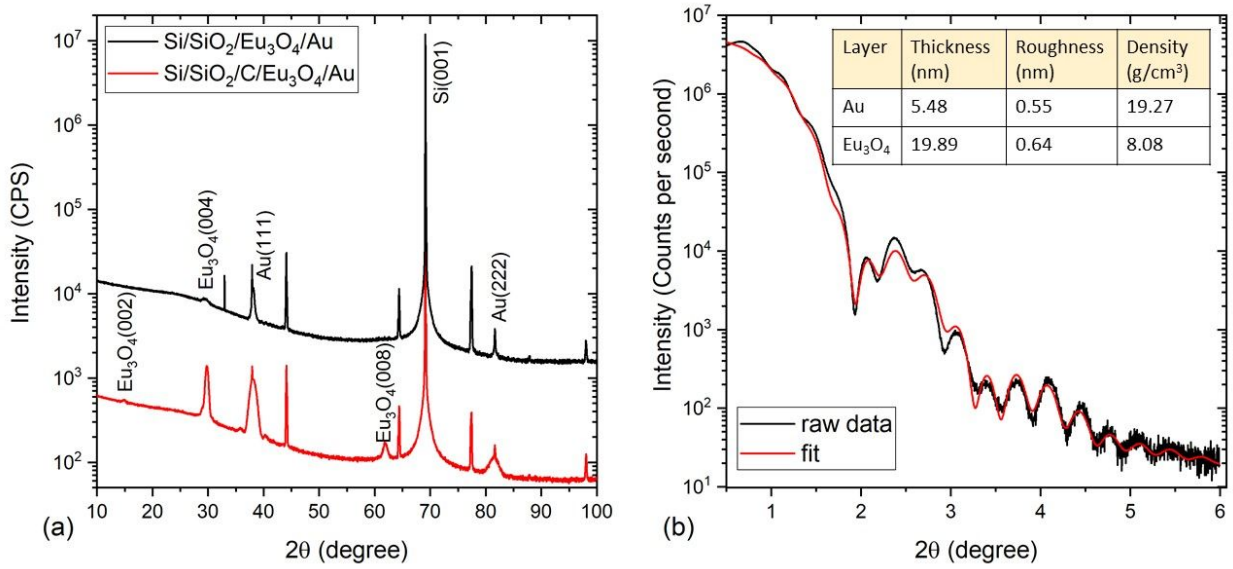


FIG. 2. (a) The RT XRD scan of $Si/SiO_2/Eu_3O_4(001)/Au$ (black line) and $Si/SiO_2/C/Eu_3O_4(001)/Au$ (red line) samples carried out between 20° - 100° using a monochromator and a 1D detector. The scan for the $Si/SiO_2/C/Eu_3O_4(001)/Au$ sample is down-shifted by a factor of five for ease of comparison. (b) The XRR measurement of the $Si/SiO_2/Eu_3O_4(001)/Au$ sample (black line) and the corresponding fit (red line). The table lists the thickness, roughness and density of the deposited films as deduced from the fit.

for impurities of Eu_3O_4 phase in EuO_{1-x} thin films which sometimes show a pronounce bump at $T < 20$ K [6, 7].

The ZFC isothermal magnetisation measurements as a function of the applied magnetic field for the $Si/SiO_2/graphene/Eu_3O_4/Au$ sample at 2 K, 5K and 10 K are shown in Figure 4. The hysteresis curves show that the grown Eu_3O_4 films exhibit ferromagnetic behaviour with a coercive field of 22 Oe. The inset highlights the virgin magnetisation curves at these temperatures. Although the XRD scans (Figure 2 (a)) and the M vs T measurements (Figure 3) prove the growth of $Eu_3O_4(001)$ thin films, surprisingly, the virgin $M-H$ curves show no metamagnetic transition even with an applied in-plane magnetic field of 3 kOe as reported for crystal and powder Eu_3O_4 [3, 4]. This could be attributed to the strain from the substrate which could be resolved by growing a thicker film.

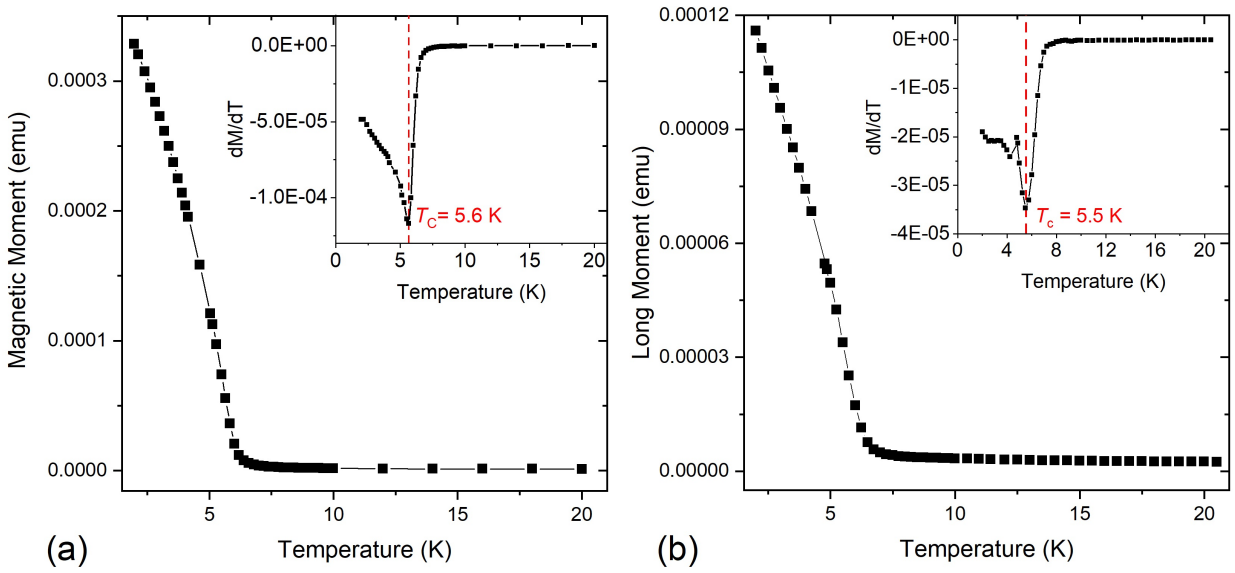


FIG. 3. (a) The 20 Oe FC M vs T measurement for $Si/SiO_2/Eu_3O_4/Au$. The inset presents the dM/dT vs T plot used to determine the T_C. (b) The ZFC M vs T measurement for the $Si/SiO_2/graphene/Eu_3O_4/Au$ sample. The inset shows the dM/dT vs T graph used to deduce the T_C of the Eu_3O_4.

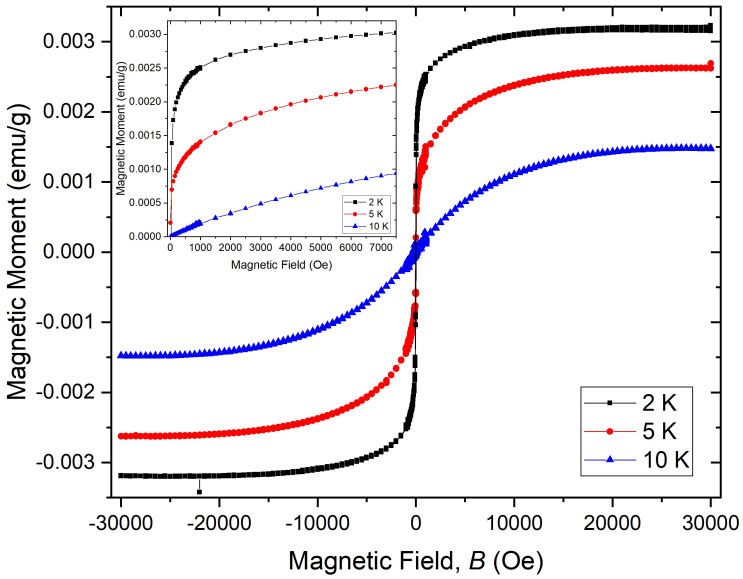


FIG. 4. ZFC Isothermal magnetisation hysteresis loops of the $Si/SiO_2/graphene/Eu_3O_4/Au$ sample measured as a function of the temperature at 2 K, 5 K and 10 K. The inset highlights the virgin magnetisation curves at these temperatures.

C. XPS

The existence of mixed-valence Eu cations was investigated by performing depth-profile XPS scans while measuring the Eu $3d$ and $4d$ spectra simultaneously after Ar^+ plasma etching. Figure 5 (a) shows the XPS etch profile of the sample, whereas the XPS survey collected at t=210 s, 360 s, 450 s and 510 s, highlighting the different detected elements are shown in Figure 5 (b). The $4d$ XPS spectra have a complicated structure (not shown) due to the strong unfilled $4f-4d$ hole interaction, whereas the $3d$ states have a weaker multiplet splitting and broader photoexcitation cross-section. Therefore, the latter is usually used to analyse the Eu XPS spectra and obtain a better estimation of the Eu initial valence [8–11].

Figure 6 (a) - (d) shows the Eu $3d$ XPS spectra after subtracting an optimised Shirley background, measured at t=210 s, 360 s, 450 s and 510 s. The peaks were deconvoluted using Gaussian-Lorentzian fitting, while the χ^2 value indicates the quality of the fit. Although the Eu_3O_4 layer was etched fully, only these scans were considered for the analysis of the Eu cation valency (the yellow shaded area of Figure 5 (a)) to minimise the effect of interdiffusion at the SiO_2/Eu_3O_4 and Eu_3O_4/Au interfaces and increase the intensity of the Eu $3d$ and $4d$ peaks.

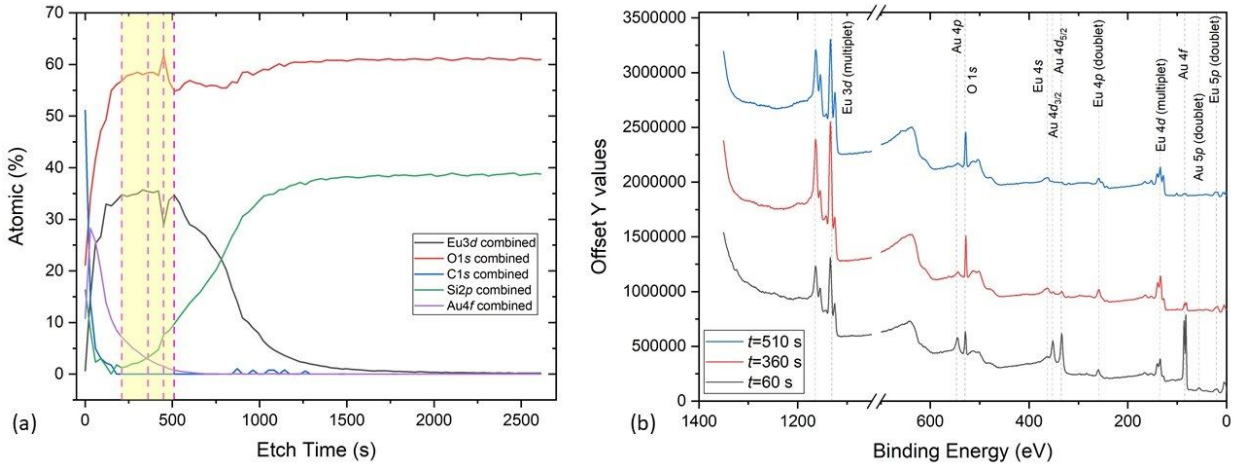


FIG. 5. (a) XPS etch profile of the $Si/SiO_2/Eu_3O_4$/Au sample by Ar^+ plasma etching. The yellow shaded region highlights the area considered for the analysis of Eu cations, whereas the dashed vertical lines indicate t =210 s, 360 s, 450 s and 510 s. (b) The XPS survey spectra collected at t= 60 s, t= 360 s and t= 510 s of the $Si/SiO_2/Eu_3O_4$/Au highlighting the Au, C, Eu, Si and O peaks.

All spectra in Figure 6 show the spin-orbit coupling (SOC) components, $3d_{5/2}$ and $3d_{3/2}$, for Eu^{2+} and Eu^{3+} separated by $\Delta \sim 29.5$ eV, which agrees with previously reported values [8, 10, 12]. They also show additional peaks at slightly higher binding energy (BE) to the SOC peaks for the Eu^{2+} and Eu^{3+}. These shake-up satellite peaks arise as a result of the multiplet structures of the $4f^7 - 3d$ hole in the final state [11]. Furthermore, the fast $3d$ photoelectrons create plasmon excitation structures observed as broad peaks at BE $\sim$ 1146 eV and $\sim$ 1170 eV [8]. The XPS spectra shown in Figure 6 prove the mixed-valency of Eu cations as they agree well with previous work reported for Eu^{2+} and Eu^{3+} [8, 10, 13–15]. Moreover, the average atomic ratio of the Eu^{2+} to Eu^{3+} in the $3d_{5/2}$ and $3d_{3/2} \sim 28 : 72$ is consistent with the values reported in Eu-doped ZnO [16] and Eu-doped GaN nanowires [17]. Table I summarises the positions of the Eu^{2+} and Eu^{3+} $3d$ peaks, their FWHM, their corresponding multiplet satellites, the ratio of Eu^{2+}/Eu^{3+} and the fits χ^2 values of the four

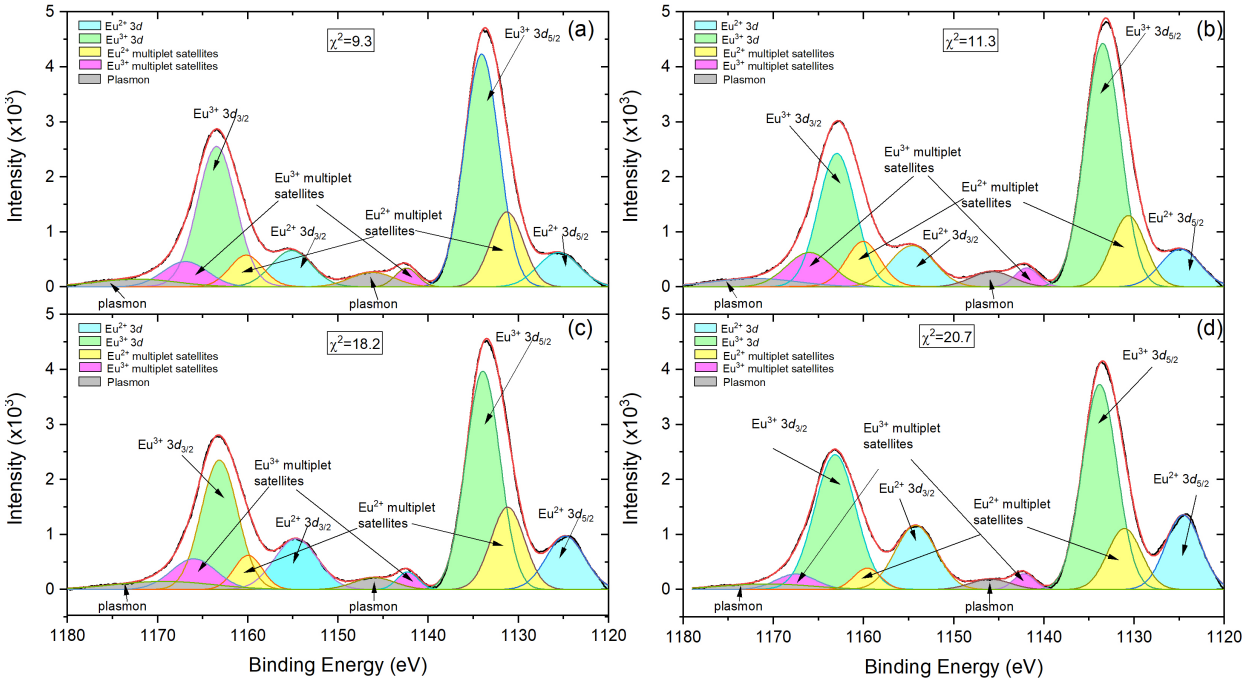


FIG. 6. The deconvoluted $3d$ XPS spectra of the Eu_3O_4 film on Si/SiO_2 substrate using Al Kα source (1486.68 eV) after the Shirley background subtraction, measured at etching time (a) t=210 s, (b) t=360 s, (c) t=450 s and (d) t=510 s. The raw data (black line), fitting curve (red line), Eu^{2+} $3d$ (blue shaded peaks), Eu^{2+} multiplet satellites (yellow-shaded peaks), $Eu^{3+}3d$ (green shaded peaks), Eu^{3+} multiplet satellites (magenta shaded peaks) and plasmon excitations (grey shaded peaks).

TABLE I. The positions of the Eu^{2+} and Eu^{3+} $3d$ peaks, their FWHM and the position of their corresponding multiplet satellites. The atomic ratios of the Eu^{2+} to Eu^{3+} were deduced from the areas of the peaks. The table also lists the χ^2 value of the fittings.

Spectrum	Eu^{2+} (eV)					
	$3d_{5/2}$	FWHM	$3d_{5/2}$ Satellites	$3d_{3/2}$	FWHM	$3d_{3/2}$ Satellites
t= 210 s	1125.54	5.39	1131.26	1155.14	5.29	1160.16
t= 360 s	1124.88	5.17	1130.64	1154.75	5.76	1160.04
t= 450 s	1124.78	5.01	1131.19	1154.65	5.64	1159.96
t= 410 s	1124.56	4.58	1131.07	1154.21	5.36	1159.58
	Eu^{3+}(eV)					
	$3d_{5/2}$	FWHM	$3d_{5/2}$ Satellites	$3d_{3/2}$	FWHM	$3d_{5/2}$ Satellites
t= 210 s	1134.07	4.56	1142.39	1163.46	5.03	1166.92
t= 360 s	1133.49	4.69	1141.90	1162.96	4.85	1166.00
t= 450 s	1133.93	4.46	1142.29	1163.15	4.80	1166.00
t= 410 s	1133.83	4.56	1142.23	1163.15	5.38	1167.48

	Atomic ratio $3d_{5/2}$		Atomic ratio $3d_{3/2}$		χ^2
	Eu^{2+}	Eu^{3+}	Eu^{2+}	Eu^{3+}	
t= 210 s	49.81	50.19	21.39	78.61	9.30
t= 360 s	14.63	85.37	26.84	73.16	11.30
t= 450 s	21.58	78.42	31.61	68.39	18.20
t= 410 s	26.80	73.20	31.96	68.04	20.70
Average	28.20	71.80	27.95	72.05	

spectra.

D. Raman Spectroscopy

Raman spectroscopy is a versatile and non-destructive technique widely used to study the structural and electronic properties of graphene [18, 19]. A good-quality monolayer of graphene has two main characteristic Raman peaks; the G and $2D$ peaks at $\sim$ 1582

cm^{-1} and $\sim$ 2700 cm^{-1}, respectively. It can also possesses other disorder-induced peaks such as the D peak at $\sim$ 1350 cm^{-1} [20–22]. Therefore, the presence or absence of these peaks and the ratio of the intensity of the D peak to the intensity of the G peak (I_D/I_G), which represents the defect density in the graphene structure, were mostly used to assess the quality of our graphene underlayer [23].

Figure 7 (a) and (b) show the microscopic optical images of the sample highlighting three different regions of the Si/SiO_2/graphene/Eu_3O_4/Au sample taken before etching the Au capping layer. The zoom-in image collected with a $\times$100 objective lens (Figure 7 (b)) shows that the graphene layer consists of a mixture of mono- and multilayer graphene domains rather than a continuous homogeneous monolayer, which could be either a result of the growth of the Eu_3O_4 film or the pristine quality of the commercial graphene. Therefore, one would expect the presence of defect-induced peaks in the Raman scans [23].

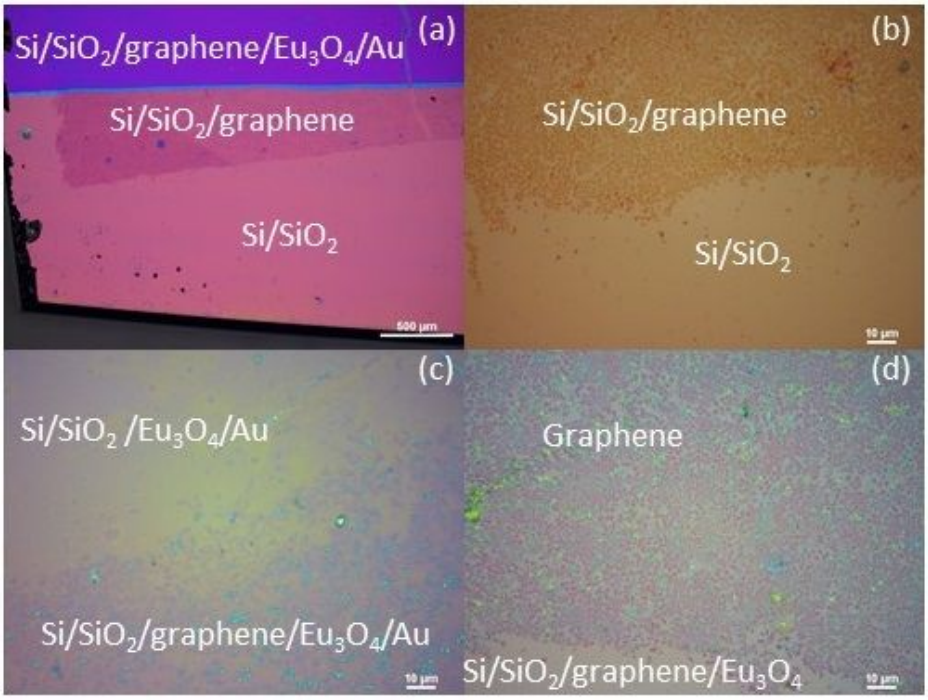


FIG. 7. The microscopic optical images of the Si/SiO_2/graphene/Eu_3O_4/Au sample highlighting the different regions of the sample. (a) the bare and coated area of the Si/SiO_2 substrate before the etching process, (b) a zoom-in view of the surface using a 100X objective lens showing the mixed domain structures of the graphene underlayer, (c) the graphene under the Eu_3O_4 layer before and (d) after etching the Au capping layer.

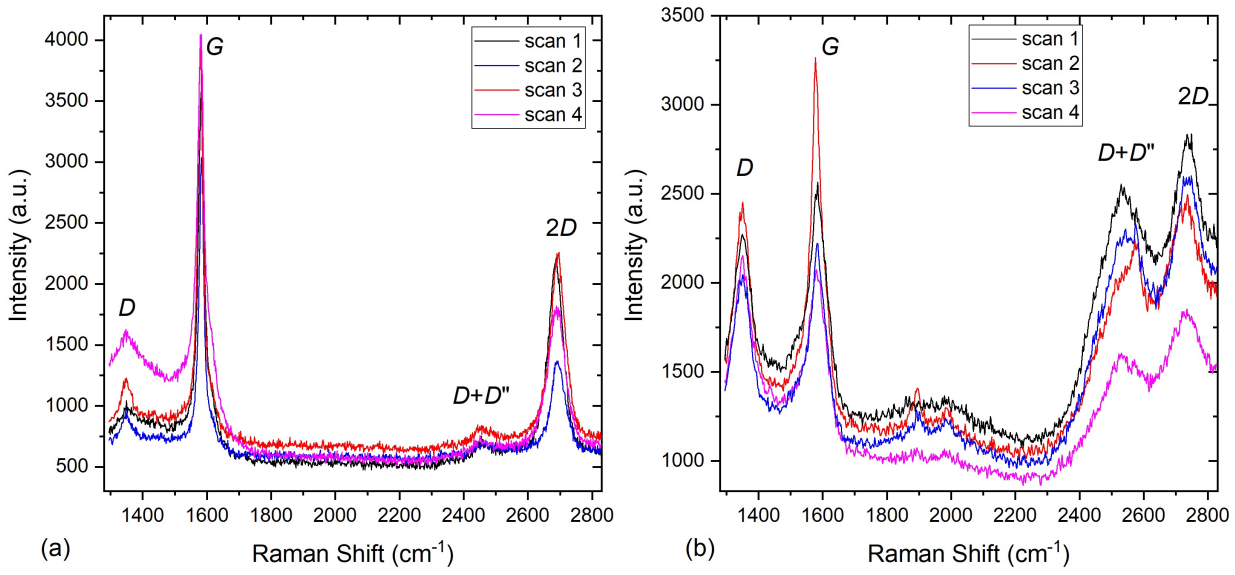


FIG. 8. RT Raman spectroscopy measurements for (a) the bare graphene sheet on the Si/SiO_2 substrate and (b) graphene under the Eu_3O_4 film after etching the Au capping layer.

Figure 7 (c) and (d) show the microscopic optical images of the graphene edge under the Eu_3O_4 film before and after removing the Au layer, respectively. No significant change in the contrast is observed between the two images suggesting that the etching process did not remove or affect the graphene underlayer.

Four random Raman scans taking on two different areas of the sample's surface; bare graphene and the graphene/Eu_3O_4 region after removing the Au layer are shown in Figure 8 (a) and (b), respectively. The emergence of the additional defect-induced peaks in the spectra of the graphene/Eu_3O_4 area and the increase in their intensities (Figure 8 (b)) compared to the scans of the bare graphene (Figure 8 (a)) indicates that the growth of Eu_3O_4 film increased the defect density in the graphene structure. This is also seen by the shift in the I_D/I_G ratio of the graphene under the Eu_3O_4 film towards the higher values, compared to the bare graphene sheet (Figure 9). This is because I_D/I_G is known to be small for low-defect-density graphene [22, 24]. However, since the underlayer graphene is visible with the optical microscope (Figure 7) and that the Raman characteristic features of graphene are maintained after the growth of the Eu_3O_4 film (Figure 8), one would expect the graphene underlayer to retain its properties.

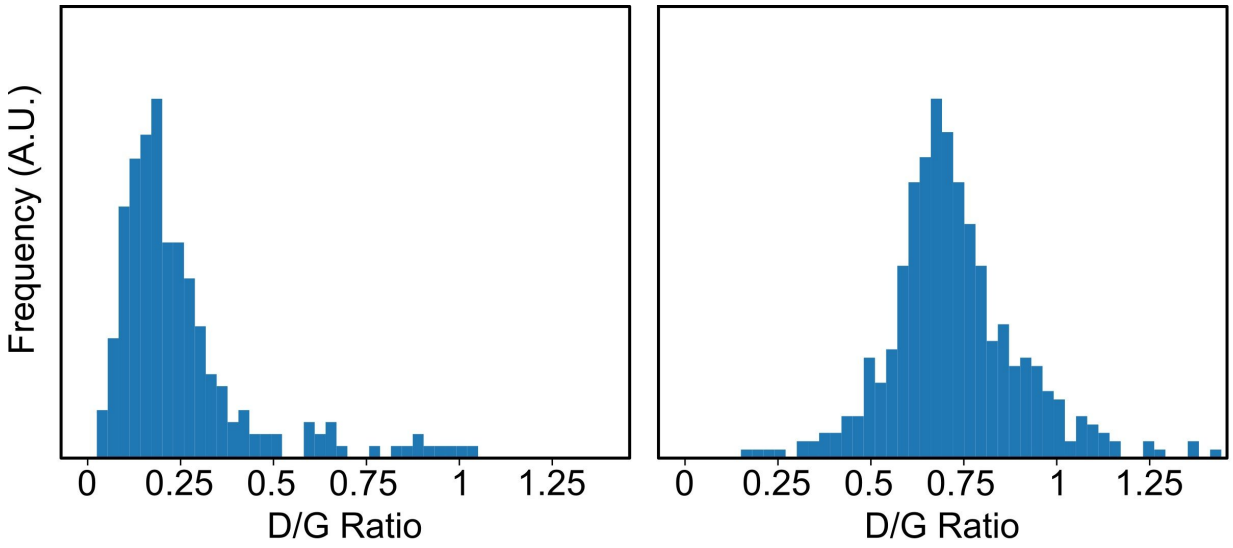


FIG. 9. The frequency distribution of the intensity of the D peak to the intensity of the G peak of (a) the bare graphene and (b) the graphene under the Eu_3O_4 film. Raman spectra of the regions with no graphene signal were removed from the statistics.

IV. CONCLUSION

In summary, we discussed the experimental work carried out to study the growth of Eu_3O_4 thin film by MBE on Si/SiO_2 and on a graphene sheet. The structural and magnetic characterisations show successful deposition of crystalline, highly-textured $Eu_3O_4(001)$ films with a T_C of $\sim 5.5 \pm 0.1$ K. However, the films show no metamagnetic behaviour which could be attributed to the strain from the substrate. Furthermore, a qualitative analysis of the XPS scans confirms the mixed-valency of the Eu cation.

Raman measurements show that the graphene layer retained its hexagonal lattice structure under the Eu_3O_4 film. Therefore, this study represents the first successful step towards integrating a Eu_3O_4 thin film in two widely used electronic substrates for future spintronics applications.

ACKNOWLEDGMENTS

Authors would like to acknowledge David Love and Pedro M S Monteiro for their support.

[1] C. M. Varma, Mixed-valence compounds, Reviews of Modern Physics **48**, 219 (1976).

[2] R. C. Rau, The crystal structure of Eu3O4, Acta Crystallographica **20**, 716 (1966).

[3] K. Ahn, V. K. Pecharsky, and K. A. Gschneidner, The magnetothermal behavior of mixed-valence Eu3 O4, Journal of Applied Physics **106**, 043918 (2009).

[4] L. Holmes and M. Schieber, Magnetic Ordering in Eu3O4 and EuGd2O4, Journal of Applied Physics **37**, 968 (1966).

[5] L. Holmes and M. Schieber, Metamagnetism in Eu3O4, Physical Review **167**, 449 (1968).

[6] P. Liu and J. Tang, Antiferromagnetic coupling in EuO1-x, Physical Review B **85**, 224417 (2012).

[7] P. Liu and J. Tang, A magnetic polaron model for the enhanced Curie temperature of EuO 1- x, Journal of Physics: Condensed Matter **25**, 125802 (2013).

[8] C. Caspers, M. Müller, A. X. Gray, A. M. Kaiser, A. Gloskovskii, C. S. Fadley, W. Drube, and C. M. Schneider, Chemical stability of the magnetic oxide EuO directly on silicon observed by hard x-ray photoemission spectroscopy, Physical Review B - Condensed Matter and Materials Physics **84**, 1 (2011).

[9] E.-J. Cho, T. Oh, S.-J. Suzuki, and T. Kasuya, Electronic structure study of Eu intermetallic compounds by photoelectron spectroscopy, Journal of Electron Spectroscopy and Related Phenomena **77**, 173 (1996).

[10] A. Mariscal, A. Quesada, A. T. Martín-luengo, M. A. García, A. Bonanni, J. F. Fernández, and R. Serna, Applied Surface Science Europium monoxide nanocrystalline thin films with high near-infrared transparency, Applied Surface Science **456**, 980 (2018).

[11] T. Cho, En-Jin and Oh, S.-J. and Imada, S. and Suga, S. and Suzuki, T. and Kasuya, Origin ofthe high-binding-energy structure in the 3d core-level spectra of divalent Eu compounds, Physical Review B **51**, 10146 (1995).

[12] B. A. Orlowski, S. Mickievicius, V. Osinniy, A. J. Nadolny, and B. Taliashvili, High-energy X-ray photoelectron spectroscopy study of MBE grown (Eu , Gd) Te layers, Nuclear Instruments

and Methods in Physics Research B **238**, 346 (2005).

[13] Y. Ohno and T. Urata, Photoelectron spectra and surface valence fluctuation of Eu in the misfit-layer compound {(EuS)1.15}1.5NbS2, Journal of Electron Spectroscopy and Related Phenomena **125**, 171 (2002).

[14] D. Kim, J. R. Jeong, Y. Jang, J.-S. Bae, I. Chung, R. Liang, D.-K. Seo, S.-J. Kim, and J.-C. Park, Self-emitting blue and red EuOX (X = F, Cl, Br, I) materials: band structure, charge transfer energy, and emission energy, Physical Chemistry Chemical Physics **21**, 1737 (2019).

[15] E. Cho and S.-J. Oh, Surface valence transition in trivalent Eu insulating compounds observed by photoelectron spectroscopy, Physical Review B **59**, 3 (1999).

[16] O. Lupan, T. Pauporté, B. Viana, P. Aschehoug, M. Ahmadi, B. R. Cuenya, Y. Rudzevich, Y. Lin, and L. Chow, Eu-doped ZnO nanowire arrays grown by electrodeposition, Applied Surface Science **282**, 782 (2013).

[17] D. N. Faye, X. Biquard, E. Nogales, M. Felizardo, M. Peres, A. Redondo-Cubero, T. Auzelle, B. Daudin, L. H. Tizei, M. Kociak, P. Ruterana, W. Möller, B. Méndez, E. Alves, and K. Lorenz, Incorporation of Europium into GaN Nanowires by Ion Implantation, Journal of Physical Chemistry C **123**, 11874 (2019).

[18] Y. Y. Wang, Z. H. Ni, Z. X. Shen, H. M. Wang, and Y. H. Wu, Interference Enhancement of Raman Signal of Graphene, Applied Physics Letters **92**, 10.1063/1.2838745 (2008), arXiv:0801.4595.

[19] I. Chilres, L. A. Jauregui, W. Park, H. Cao, and Y. P. Chen, Raman Spectroscopy of Viruses and Viral Proteins, in *New Developments in Photon and Materials Research*, edited by J. I. Jang (Nova Science Publishers, Incorporated, 2013) Chap. 19, pp. 553–595.

[20] A. Allard and L. Wirtz, Graphene on Metallic Substrates: Suppression of the Kohn Anomalies in the Phonon Dispersion, Nano Letters **10**, 4335 (2010).

[21] L. M. Malard, M. A. Pimenta, G. Dresselhaus, and M. S. Dresselhaus, Raman Spectroscopy in Graphene, Physics Reports **473**, 51 (2009).

[22] I. Shlimak, A. Haran, E. Zion, T. Havdala, Y. Kaganovskii, A. V. Butenko, L. Wolfson, V. Richter, D. Naveh, A. Sharoni, E. Kogan, and M. Kaveh, Raman Scattering and Electrical Resistance of Highly Disordered Graphene, Physical Review B **91**, 045414 (2015).

[23] R. O. M. Aboljadayel, D. M. Love, C. A. F. Vaz, R. S. Weatherup, P. Braeuninger-Weimer, M. B. Martin, A. Cabrero-Vilatela, A. Ionescu, C. J. Kinane, T. R. Charlton, J. Llandro,

P. M. S. Monteiro, C. H. W. Barnes, S. Hofmann, and S. Langridge, Determining the Proximity Effect Induced Magnetic Moment in Graphene by Polarised Neutron Reflectivity and X-ray Magnetic Circular Dichroism, , 1 (2021), arXiv:2101.09946.

[24] A. Cabrero-Vilatela, R. S. Weatherup, P. Braeuninger-Weimer, S. Caneva, and S. Hofmann, Towards a General Growth Model for Graphene CVD on Transition Metal Catalysts, Nanoscale **8**, 2149 (2016).